

PAPER

## Effect of sawtooth crashes on fast ion distribution in NSTX-U

To cite this article: D. Liu *et al* 2018 *Nucl. Fusion* **58** 082028

View the [article online](#) for updates and enhancements.

### Related content

- [Study of the effect of sawteeth on fast ions and neutron emission in MAST using a neutron camera](#)  
M Cecconello, A Sperduti and the MAST team
- [Orbit modeling of fast particle redistribution induced by sawtooth instability](#)  
D. Kim, M. Podestà, D. Liu *et al.*
- [Energetic particles in spherical tokamak plasmas](#)  
K G McClements and E D Fredrickson

### Recent citations

- [Orbit modeling of fast particle redistribution induced by sawtooth instability](#)  
D. Kim *et al*

# Effect of sawtooth crashes on fast ion distribution in NSTX-U

D. Liu<sup>1,3</sup>, W.W. Heidbrink<sup>1</sup>, M. Podestà<sup>2</sup>, G.Z. Hao<sup>1</sup>, D.S. Darrow<sup>2</sup>, E.D. Fredrickson<sup>2</sup> and D. Kim<sup>2</sup>

<sup>1</sup> Department of Physics and Astronomy, University of California-Irvine, Irvine, CA 92697, United States of America

<sup>2</sup> Princeton Plasma Physics Laboratory, Princeton, NJ 08543, United States of America

E-mail: [deyongl@uci.edu](mailto:deyongl@uci.edu)

Received 4 December 2017, revised 30 April 2018

Accepted for publication 21 May 2018

Published 3 July 2018



CrossMark

## Abstract

During the 2016 experimental campaign of NSTX-U (Menard *et al* 2012 *Nucl. Fusion* **52** 083015), long L-mode and reproducible sawtooth plasmas have been achieved that were previously not accessible before the upgrade. This provides a good opportunity to study the effect of sawtooth crashes on fast ion confinement and redistribution in spherical tokamaks. The solid-state neutral particle analyzer (SSNPA) and fast ion D-alpha (FIDA) diagnostics on NSTX-U each have a tangentially-viewing instrument and a radially- or vertically-viewing instrument, which are mainly sensitive to passing and trapped fast ions, respectively. It has been observed on both diagnostics that passing particles are strongly expelled from the plasma core to the edge during sawtooth crashes, while trapped fast ions are weakly affected. The tangentially-viewing SSNPA observes large signal spikes at the sawtooth crashes because fast ions move to the edge and charge exchange with edge neutrals. The radially-viewing SSNPA data suggest that there is a small drop of trapped particles in the core. The tangentially-viewing FIDA (t-FIDA) system observes a depletion as large as 25% in the region inside the inversion radius, while an increase at the outer region. There is almost no change in the signals of the vertically-viewing FIDA system. The neutron emission can drop as much as 15% at the sawtooth crashes, accompanied by an increase of edge  $D_\alpha$  light. Simulations with the Kadomtsev and Porcelli sawtooth models have been performed and compared with the measurements. The full reconnection Kadomtsev model overestimates the neutron rate drop at each sawtooth crash. When tuning the sawtooth input parameters, the partial reconnection Porcelli sawtooth model can qualitatively reproduce the neutron rate drop and t-FIDA signal drop in the core, but it fails to predict the t-FIDA signal increase at the edge.

Keywords: sawtooth, fast ion, spherical tokamak

(Some figures may appear in colour only in the online journal)

## 1. Introduction

Sawtooth crashes are periodic collapses of central plasma temperature followed by slow recoveries when the safety factor  $q$  at the magnetic axis,  $q_0$ , drops below unity. After it was first discovered by Von Goeler *et al* in 1974 [1], sawtooth crashes have been observed in nearly every tokamak device. Generally, sawteeth moderately degrade the plasma

confinement. Large amplitude sawtooth crashes can trigger neoclassical tearing modes [2], which can further degrade the plasma confinement and lead to a plasma disruption. Regulated small sawtooth oscillations could be beneficial in flushing impurities from the plasma core. Sawtooth crashes also cause transport of fast ions, which are an important portion of the plasma energy and the current drive. A significant redistribution of fast ions can change their interaction with the background plasma and affect fast ion confinement and MHD instabilities, including the sawtooth instability itself.

<sup>3</sup> Author to whom any correspondence should be addressed.

It is important to understand the effect of sawtooth crashes on the fast ion population and develop a coherent sawtooth control strategy to take account of the alpha particles and fast ions. In this paper, we mainly focus on the effect of sawtooth crashes on the fast ion distribution.

Sawteeth were observed to cause significant fast ion transport in TFTR [3] and JET [4] as evident from neutron rate drop. Recent experiments on TEXTOR [5], DIII-D [6], and ASDEX Upgrade [7–9] show that in conventional tokamaks passing fast ions are much more susceptible to sawtooth-induced transport than trapped particles. The DIII-D experimental data also suggest that the redistribution of trapped fast ions may have some energy dependence. All these observations qualitatively agree with the Kadomstev sawtooth model [10, 11]. In the Kadomstev model, a sawtooth crash is essentially a magnetic reconnection process in which a fast change of helical magnetic flux and a large electric field are induced. The simulations with the Kadomstev model can reproduce the trend observed in experiments, but there is some discrepancy in the magnitude of the change [6]. However, the effect of sawtooth crashes on the fast ion distribution in spherical tokamaks is much less studied due to difficulties of interpretation and a limited number of spherical tokamaks with strong auxiliary heating systems. Recent fast ion D-alpha (FIDA) measurements on MAST indicate that sawteeth induce a small redistribution of high energy passing particles in the mid-radius and a reduction of the trapped fast ion population at all energies in the plasma core [12]. The neutron camera (NC), which is most sensitive to fast ions close to the injection energy, observes that there is a 50% reduction of neutron emission in the plasma core [13]. Modelling with different sawtooth models are all in agreement with the NC measurements; the data cannot distinguish among different sawtooth models. It is concluded that passing and trapped particles are affected in a similar level in the MAST. This is quite different from the observations presented in this paper, i.e. passing fast ions are strongly redistributed by the sawtooth crash, while trapped particles are weakly affected.

In principle, sawteeth in spherical tokamaks could be significantly different from those in conventional tokamaks. First, because of the relatively low magnetic field and compact machine size of spherical tokamaks, fast ions born from neutral beam injection often have very large gyroradius. Depending on the energy and pitch angle, the gyroradius can be a significant fraction of plasma minor radius, and it is in the same order as the sawtooth mixing radius. For example,  $\rho/a$  in the spherical tokamak NSTX [14] can be as large as 0.3 for typical beam injection energies of 80–90 keV, where  $\rho$  is the fast ion gyroradius and  $a$  is the minor radius. The ratio of the gyroradius to machine size in the existing spherical tokamaks is also comparable to the ratio of alpha-particle gyroradius to machine size in future spherical tokamak D-T reactors. The finite Larmor radius (FLR) effect on sawtooth is not thoroughly studied. Secondly, the thermal ions in spherical tokamaks also have much larger gyroradius than those in conventional tokamaks, which may affect the magnetic reconnection at the sawtooth crashes. The current sheet thickness in the magnetic reconnection is generally believed to scale with

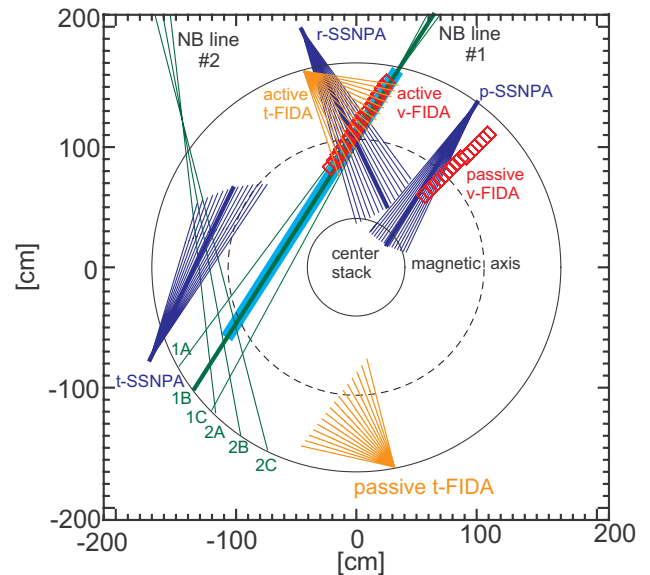


**Figure 1.** Plan view of the NSTX-U vessel with neutral beam centerlines, tangential- and vertical-FIDA sightlines, tangential-, radial- and passive-SSNPA sightlines. The original NSTX beams are labeled 1A, 1B and 1C, and the three new beam sources are labeled 2A, 2B and 2C. In most discharges analyzed in this paper, only the neutral beam source 1B is used, and the shaded light blue region represents the nominal beam width. The normal directions for the plasma current and toroidal field are counter-clockwise and clockwise, respectively.

ion gyro-radius. Thirdly, the  $q$  profile in spherical tokamaks is often observed to have  $q \approx 1$  over quite a large radius. The low magnetic shear could also alter the sawtooth behavior. Moreover, spherical tokamaks generally have higher values of  $\beta$  (the ratio of bulk plasma pressure to the magnetic field pressure) and a larger population of fast ions compared with conventional tokamaks. There could be some competition and interplay between sawtooth instability and other low-frequency instabilities such as fishbones and kinks. Therefore, sawtooth studies in spherical tokamaks complement studies in conventional high field tokamaks by providing data in a different plasma parameter regime, thereby promoting sawtooth model development and code validation, and are useful for studying alpha particles in spherical tokamak reactors.

The National Spherical Torus eXperiment Upgrade facility (NSTX-U) [15–17] is a mid-size spherical tokamak with toroidal field  $B_T(0)$  up to 1 T, plasma current  $I_p = 1.0$ – $2.0$  MA and aspect ratio  $R/a = 1.6$ – $1.8$ . The NSTX-U completed its first plasma operational campaign [18] in the summer of 2016 after it completed two main upgrades from NSTX [14]: (1) a new and larger center stack that enables higher toroidal field current (hence higher  $B_t$ ) and three times larger ohmic flux, which can approximately double the toroidal magnetic field and plasma current, and (2) three outboard neutral beam sources with tangency radii  $R_{\text{tan}} = 1.3$ , 1.2, and 1.1 m (labeled 2A, 2B, and 2C, respectively) in addition to the existing three inboard neutral beam sources from NSTX with  $R_{\text{tan}} = 0.7$ , 0.6, and 0.5 m, (labeled 1A, 1B, and 1C, respectively), as shown in figure 1. These three new outboard beam sources aim at increasing the available auxiliary heating power and neutral beam driven current and expanding the flexibility in fast ion

pressure, rotation and  $q$  profile control. The total neutral beam injection power is increased from 6 MW to 10 MW. In the NSTX-U's 2016 campaign, 2 s long L-mode sawtooth discharges that had not been available on NSTX were routinely achieved [19]. Although the sawtooth discharges in this paper are obtained from the NSTX-U commissioning phase, the main fast ion diagnostics that will be described in section 2 already worked properly. These sawtooth shots provide a good database to study the effect of sawtooth crashes on fast ion distribution in spherical tokamaks.

The main purpose of this work is to present experimental observations of sawtooth effects on fast ion distribution in NSTX-U and compare with the sawtooth modelling of TRANSP/NUBEAM code [20, 21]. The paper is organized as follows. The plasma conditions and main fast ion diagnostics are firstly described in section 2. Then the experimental setup and fast ion diagnostic measurements during the sawtooth crashes are presented. Measurements from multiple fast ion diagnostics confirm that sawtooth crashes affect passing and trapped fast ions differently. Section 3 compares the TRANSP sawtooth simulations with experimental measurements. The full reconnection Kadomtsev model [10, 11] and a partial reconnection Porcelli model [22] have been used in the simulations. In addition, the critical energies for redistribution of passing and trapped fast ions based on Kolesnichenko's theory [23–25] are calculated. They can explain the experimental observations on the different behavior of passing and trapped particles reasonably well. Finally, section 4 summarizes the conclusions of this study and on-going work.

## 2. Experimental setup and measurements

The fast ion distribution function is a complicated function in phase space. Its deposition requires at least two dimensions in real space and two dimensions in velocity/energy. Therefore, multiple diagnostics are often needed to diagnose the fast ion distribution. The fast ion diagnostic suite on NSTX-U consists of neutron detectors, solid state neutral particle analyzer (SSNPA) arrays [26, 27] and fast ion D-alpha (FIDA) spectroscopy [28, 29]. Unfortunately, the scintillator-based fast loss ion probe (sFLIP) [30, 31] and the charged fusion product diagnostic [32, 33] were not ready for the run campaign, and there are no direct measurements of fast ion loss for this study. The neutron detectors measure the volume-integrated neutron flux. They provide a good indicator of high energy fast ions in the plasma core since beam-target reactions are the dominant fusion reactions on NSTX-U.

Figure 1 shows the SSNPA and FIDA detector locations and sightlines projected onto the equatorial plane of the NSTX-U vessel. The newly developed SSNPA diagnostic is a compact solid state neutral particle analyzer (NPA) based on silicon photodiodes. It measures neutral particle fluxes resulting from charge exchange (CX) reactions between fast ions and neutrals. The CX reactions are either with neutrals from neutral beam injection or with cold neutrals that penetrate into the plasma from the edge. The former process is called active CX, while the latter is called passive CX. The escaping neutral

velocity is determined by the fast ion velocity at the time of the CX reaction. Since the CX region is generally localized to the beam footprint (plasma edge) for active (passive) signal and since only neutrals moving along the line of sight can be detected, each NPA detector (especially active NPA) measures a relatively narrow range of velocity pitch angles. These relatively localized measurements in phase space are a valuable complement to techniques that average over pitch angles, such as neutron and FIDA diagnostics.

The SSNPA instrument on the NSTX-U consists of three 16-channel silicon photodiode arrays stacked vertically. A relatively large aperture is employed in the SSNPA system so that a neutral particle flux instead of individual particles is measured by the detector. In this so-called current mode of operation (as opposed to pulse-counting mode), the SSNPA can have high a temporal resolution by sacrificing energy resolution. In order to obtain some energy resolution, the three arrays are coated with thin foils of different thickness; energy loss in the foils determines the minimum energy detected in each array. To obtain a spatial profile from active charge-exchange measurements, the sightlines of the arrays are oriented to intersect a heating neutral beam. One instrument, labeled t-SSNPA, is oriented to measure ions with large tangential velocity components and has sightlines that intersect the more tangential 2A, 2B, and 2C sources. Another instrument, named r-SSNPA, is oriented to measure neutrals with large radial velocity components and has sightlines that intersect the more perpendicular 1A, 1B, and 1C sources. In addition, a similar instrument with only one silicon photodiode array is oriented radially with sightlines that miss all heating beams; it monitors the passive signal and is called p-SSNPA. The SSNPA diagnostic worked very well on NSTX-U in the 2016 campaign; it can detect fluctuations up to 120 kHz with a sampling rate of 500 kHz. The energy threshold for the three different thickness (100 nm, 200 nm and 300 nm) foils are >25 keV, >45 keV, and >65 keV respectively.

The FIDA diagnostic is an application of charge-exchange recombination spectroscopy [34]. It measures the Doppler-shifted  $D_\alpha$  emission of re-neutralized fast deuterons which have undergone CX reaction with beam neutrals or background neutrals. The light is collected by optical fibers and then sent to a spectrometer, and spectral resolution is obtained by dispersion of a bandpass-filtered portion of the light. The spectrum of FIDA light provides useful information about the distribution of fast ion velocity along the sightline. To get the FIDA spatial profile, the FIDA spectra from each radial sightline are integrated over a particular wavelength (or energy) range of interest. Similar to the SSNPA diagnostic, FIDA light can come from active signals when the CX reaction is with injected beam neutrals, and from passive signals when the CX reaction is with background neutrals, especially edge neutrals. There are currently two sets of FIDA diagnostics on NSTX-U: a toroidally viewing FIDA (labeled t-FIDA) from a lens mounted slightly above the vessel midplane, and a vertically viewing FIDA (named v-FIDA) from two lenses mounted on the top of the machine that look vertically downwards at the centerline of neutral beam source 1B. Both FIDA systems have 16 active fibers, and the intersection points with the centerline of neutral

beam source 1B are nominally the same for the t-FIDA and v-FIDA systems. The 16 fibers cover the full extent of the outboard and part of the inboard plasma region from  $R_{\text{maj}} = 85$  cm to  $R_{\text{maj}} = 155$  cm, where  $R_{\text{maj}}$  is the major radius at which the sightlines intersect the neutral beam. The intrinsic spatial resolution of the FIDA diagnostic is about 2 cm [34]. At the intersection with the midplane, both t-FIDA and v-FIDA fibers are separated radially by around 5 cm with the t-FIDA spot size varying from 2 cm to 2.5 cm in diameter from the edge to the core, and the v-FIDA spot size about 0.8 cm in diameter. The temporal resolution is 10 ms. Background subtraction is critical for the FIDA diagnostic. Each FIDA system has 16 toroidally-displaced passive (or reference) views to monitor background or passive emissions. It has also been recently observed that the cold  $D_\alpha$  light scattered in the optical system and localized/reflected emission inside the vacuum vessel can contaminate the baseline of the FIDA spectra [35]. To reduce the effect of scattered light on the FIDA spectra, a scattering correction [35] based on singular value decomposition (SVD) has been employed in the data analysis. The uncertainties due to the scattering correction are of the same order as the statistical error, and it is included in the error bars in all the FIDA data shown in this paper.

The sawtooth events analyzed in the paper are obtained from the NSTX-U deuterium discharges with a flat-top plasma current of  $I_p = 700$  kA and a toroidal magnetic field of 0.65 T at the magnetic axis ( $R_0 \approx 1.05$  m). These discharges are low density L-mode discharges which are very suitable for FIDA and SSNPA diagnostic measurements. Figure 2 shows the spectrogram of Mirnov coil signals and time traces of injected neutral beam power and neutron rate in a typical sawtoothing discharge with shot number 204163. Only the neutral beam source 1B is used to heat the plasma. The injected neutral beam power is  $P_{\text{inj}} = 1.1$  MW with injection energy of  $E_{\text{inj}} = 72$  keV. The core electron density and temperature are of order of  $2.0 \times 10^{19}$  cm $^{-3}$  and 1.5 keV respectively. The discharge has repetitive sawtooth crashes between 0.5 and 1.5 s. Although the motional Stark effect (MSE) diagnostic was not available for  $q$ -profile measurement, the instabilities are identified as sawtooth crashes based on two facts: (1) the electron temperature is observed by the multi-point Thompson scattering and x-ray diagnostics to be flattened in the plasma core after the crashes; and (2) there are  $n = 1$  signals in Mirnov spectrogram where  $n$  is the toroidal mode number.

Because only the neutral beam source 1B is used in this discharge, the r-SSNPA, active t-FIDA and v-FIDA systems detect both active and passive signals, while the t-SSNPA and p-SSNPA measure purely passive signals from the plasma edge. Figure 3 compares the velocity sensitivity or weight function of different FIDA and SSNPA systems. As indicated in figure 4, the trapped/passing boundary in energy/pitch space is typically in the region with pitch of 0.5–0.7, depending on the location. It is clearly shown that the t-FIDA and t-SSNPA are mainly sensitive to passing fast ions, and the v-FIDA, r-SSNPA, and p-SSNPA are mostly sensitive to trapped particles.

Figure 5 shows the temporal evolution of key plasma parameters related to the fast ion population and MHD activity in the discharge 204163. As shown in figure 5(b), a sawtooth

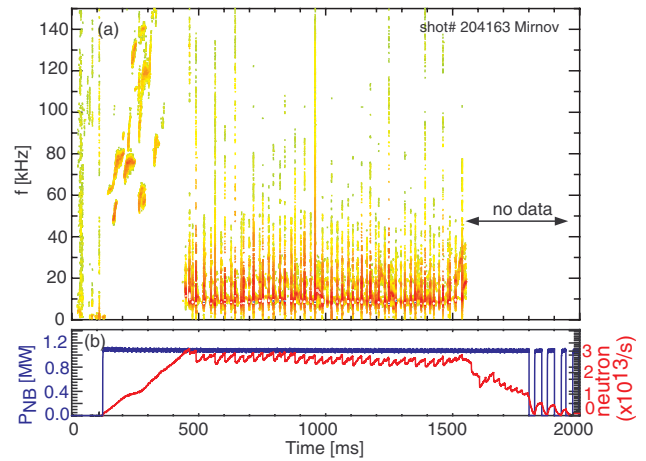


**Figure 2.** (a) Spectrogram of Mirnov coil signals and (b) temporal evolution of neutron rate and neutral beam injection power. Repetitive sawtooth crashes occur between 0.5 and 1.5 s. In addition to the dominant sawteeth, there are some weak  $n = 1$  kink or tearing modes between sawteeth.

crash can result in as large as a 15% drop of the neutron yield, implying a significant fast ion redistribution or fast ion losses. The  $D_\alpha$  radiance from the edge of the plasma also shows a spike right after every sawtooth crash. The spikes in edge  $D_\alpha$  emission indicates a loss of thermal or fast ions from the main plasma arriving at the plasma boundary. The SSNPA diagnostic has observed clear effects of sawtooth crashes on the fast ions. The effect of individual sawtooth events on the SSNPA signals is readily seen in the time traces in figures 5(c)–(e). The p-SSNPA, mainly sensitive to passive signals from trapped particles at the edge, observes a small signal increase at each sawtooth crash. The t-SSNPA, mainly sensitive to passive signals from passing particles near the edge, observes a big spike at each sawtooth crash. This is likely because passing fast ions are redistributed to the edge and charge exchange with edge neutrals. The r-SSNPA views the heating beam 1B, and the signal is the combination of the active signal from the core and the passive signal from the edge. The r-SSNPA signal shows a small depletion at each sawtooth crash. Considering that the passive signal from trapped particles slightly increases at each sawtooth crash as indicated by figure 5(c), the active signal of the r-SSNPA from trapped particles is inferred to drop at the sawtooth crashes.

All the sawtooth events in the discharge 204163 between 0.5 and 1.5 s are combined into one database to quantify the correlation between the SSNPA signal change and neutron rate drop at sawtooth crashes. Because the neutron emission in NSTX-U is dominated by beam-plasma reactions, the drop of the neutron rate at a sawtooth crash is used as an indicator of how much fast ions are affected by the sawtooth. The interpretation of the SSNPA signals is more complex since the SSNPA signal is the line integral of the product of fast ion density and neutral density along the sightline. A change of the SSNPA signal could be because of the change of fast ion density, neutral density, or the combination of both. In this work the edge  $D_\alpha$  signal is employed to estimate the edge neutral density variation. As shown in figure 6, the relative change of the p-SSNPA signal at sawtooth crashes, which is

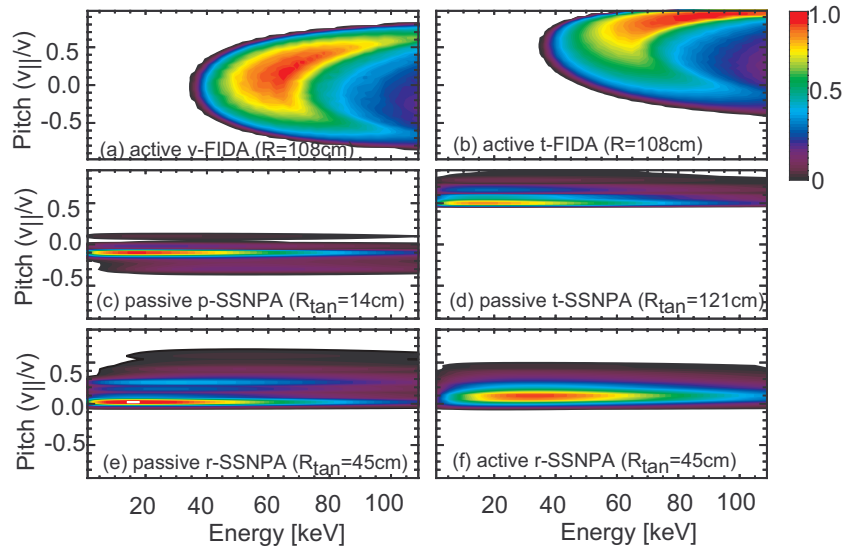


**Figure 3.** Velocity-space sensitivity functions of (a) the v-FIDA active sightline at  $R = 108$  cm and  $E_\lambda = (36.5, 68.5)$  keV, (b) the t-FIDA active sightline at  $R = 108$  cm and  $E_\lambda = (36.5, 68.5)$  keV, (c) the passive signal of the p-SSNPA channel at  $R_{\text{tan}} = 14$  cm, (d) the passive signal of the t-SSNPA channel at  $R_{\text{tan}} = 121$  cm, (e) the passive signal of the r-SSNPA at  $R_{\text{tan}} = 45$  cm and (f) the active signal of the r-SSNPA at  $R_{\text{tan}} = 45$  cm. The plotted SSNPA channels are highlighted in bold lines in figure 1. Color scale is normalized to the maximum value in each panel. Note that the FIDA and NPA diagnostics have different degrees of sensitivity in energy/pitch space. The FIDA diagnostic is sensitive to a broad strip in velocity space, while the NPA diagnostic is much more localized in pitch with a full width at half maximum (FWHM) typically less than 0.2.

defined as the ratio of the signal change at/during the sawtooth crash to the signal before the sawtooth crash, follows exactly the same trend as the edge  $D_\alpha$  signal. It suggests that the change of the p-SSNPA signal at sawtooth crashes is mainly due to the change of edge neutral density. Please note that the p-SSNPA does not intersect with any neutral beam footprint. The signal mainly comes from the edge simply because the neutral density is orders of magnitude higher in the edge than in the plasma core. Figure 6 clearly shows that the t-SSNPA signal at sawtooth crashes increases much more rapidly with the neutron rate drop, compared with the edge  $D_\alpha$  signal. The t-SSNPA signal can increase as much as a factor of 2 when the neutron rate drop is close to 15%. Since the change rate (i.e. the slope) of the t-SSNPA signal is one order of magnitude larger than that of the  $D_\alpha$  signal, it suggests that passing fast ions are strongly expelled from the core to the edge. It should be noted that the t-SSNPA also does not intersect with any neutral beam in this case and its signal is mainly from the passing fast ions near the edge. One valuable feature of the SSNPA diagnostic on NSTX-U is that there are three vertically stacked arrays viewing the similar plasma region with different filter thickness. This setup makes the SSNPA have not only high temporal resolution but also some coarse energy information. It is interesting to observe that in figure 6, all the arrays of t-SSNPA have the same trend, which suggests that a wide energy range of passing fast ions are affected by the sawtooth. In contrast, the r-SSNPA observes a small signal drop at sawtooth crashes, which indicates that there actually is some depletion of trapped particles in the plasma core. There are at least 15 low-density L-mode discharges showing similar observations as the typical case shown above.

The effect of individual sawtooth crashes on the active FIDA signal is blurred by imperfect background subtraction

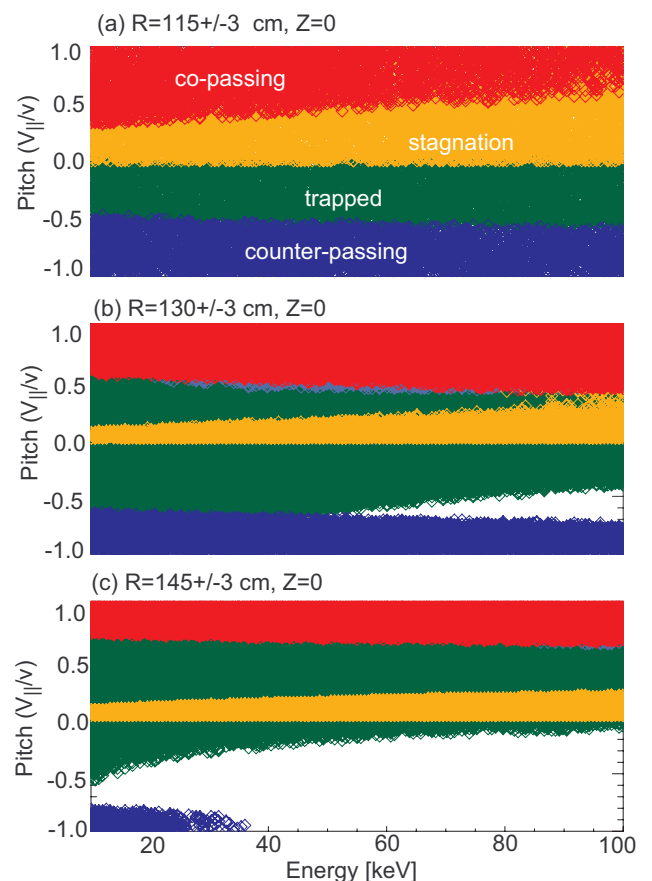


**Figure 4.** Orbit topologies in energy/pitch space at three different radial locations in the midplane. (a)  $R = 115$  cm,  $Z = 0$  (near the plasma core), (b)  $R = 130$  cm,  $Z = 0$  and (c)  $R = 145$  cm,  $Z = 0$  (near the plasma boundary). The light blue color in panel (b) represents the region with potato orbits.

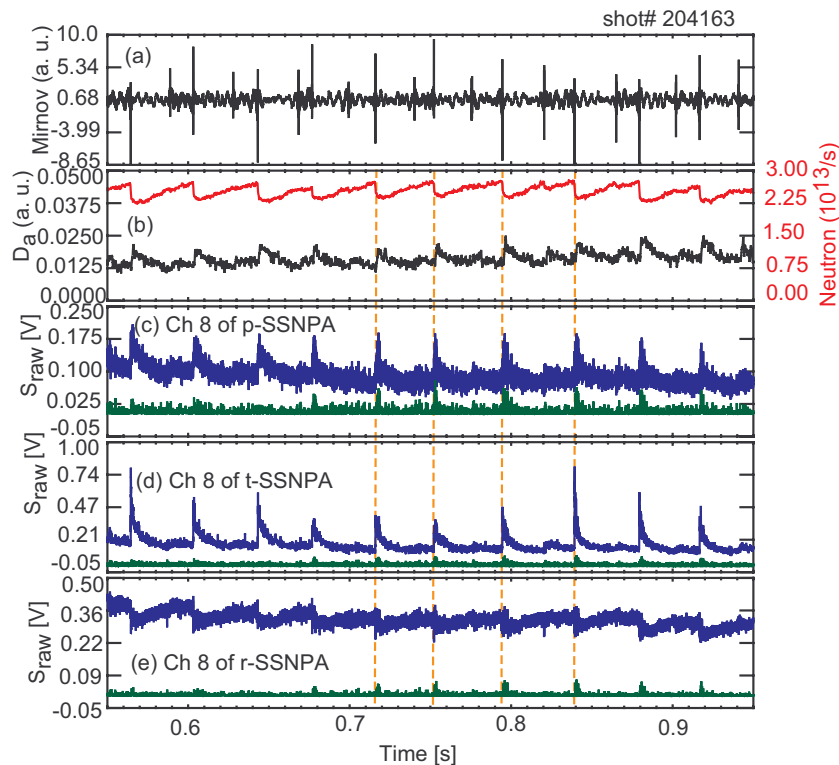


**Figure 5.** Temporal evolution of (a) Mirnov coil signals, (b) neutron emission and  $D_\alpha$  radiance from the edge of the plasma, (c) signal of channel 8 ( $R_{\text{tan}} = 14$  cm) of passive-SSNPA, (d) signal of channel 8 ( $R_{\text{tan}} = 121$  cm) of tangentially-viewing SSNPA and (e) signal of channel 8 ( $R_{\text{tan}} = 45$  cm) of radially-viewing SSNPA. In each detector array, one detector is blocked as a ‘blind’ detector to monitor EM noise and neutron induced noise. The signals on those ‘blind’ detectors are also shown in green curves in (c)–(e). The dashed vertical lines mark the time at which a sawtooth crash occur. The plotted SSNPA channels are highlighted in bold lines in figure 1. Note the different range of y-axis for panels ((c)–(e)).

because of large passive contributions, scattering of cold  $D_\alpha$  light inside the FIDA optical system and possible light reflection and localized emission from the in-vessel tiles [35]. A scattering correction and conditional averaging over several sawtooth events are employed to extract useful information from the relatively noisy FIDA data. Figures 7(a) and (b) compare the active t-FIDA spectra before and after the sawtooth crashes for two channels, one channel in the core with  $R_{\text{maj}} = 108$  cm and the other channel at the region outside of the inversion radius with  $R_{\text{maj}} = 135$  cm, where  $R_{\text{maj}}$  is the major radius that the t-FIDA sightline intersects with the neutral beam 1B centerline. The active FIDA signal is obtained by subtracting the signal in the reference view from the signal in the active view. This removes the contribution from passive FIDA light and bremsstrahlung emission. The FIDA portion of the spectrum is the Doppler-shifted region in the spectra with wavelengths from 651 nm to 653.4 nm, where the corresponding fast ion energies parallel to the sightline are 57 keV and 15 keV respectively. As shown in figures 7(a) and (b), the t-FIDA signal shows a depletion in the core channel, but an increase at the outer channel. The whole Doppler-shifted wavelength region is affected. Figure 7(c) compares the t-FIDA spatial profile before and after the sawtooth crashes, and figure 7(d) shows the change of the t-FIDA signals. A significant reduction occurs inside  $R_{\text{maj}} = 125$  cm and an increase occurs in the t-FIDA outer channels. It is worth mentioning that this inversion in the t-FIDA profile is

approximately consistent with the sawtooth inversion radius estimated from the measurements of soft x-ray emission, electron temperature and toroidal rotation. Note that in principle the thermal plasma profile evolution due to sawtooth crashes could also alter the FIDA signal and spatial profile because it can change the local beam neutral density and beam deposition. However, the FIDA synthetic modeling in section 3 suggests that the thermal plasma profile evolution and beam ion deposition change would decrease the FIDA signal at the outer region and have almost no effect on the FIDA signals with  $R < 115$  cm. Figures 7(c) and (d) show a nearly opposite trend. This enhances the statement that the observed reduction in the core and the increase at the outer region in figure 7 are mainly due to the modification of the fast ion distribution. For the v-FIDA system, little change is observed in the FIDA spectra before and after the sawtooth crashes and the data are not shown. The changes on the t-FIDA and v-FIDA signals before and after the sawtooth crashes confirm the SSNPA observations that passing particles are strongly redistributed from the core to the edge, while trapped particles are hardly affected.

Data from the innermost and outermost channels of the t-FIDA arrays are omitted in figure 7. After background subtraction, channels at the edge of the array have unphysical negative values. Generally on NSTX-U, these edge channels are more prone to background errors than the central chords [35]. Although the data shown in figure 7 appear reasonable,

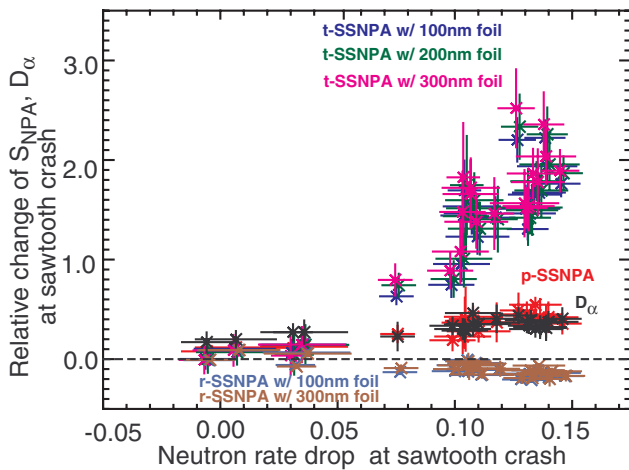


**Figure 6.** Comparison of the relative change of the edge  $D_\alpha$  and the SSNPA signals versus the neutron rate drop at/during the sawtooth crashes. The relative change of the SSNPA signal is defined as  $(S_{\text{sawtooth}} - S_{\text{pre}})/S_{\text{pre}}$ , where  $S_{\text{pre}}$  is the averaged signal in the time window of  $(-0.5, 0)$  ms relative to a sawtooth and  $S_{\text{sawtooth}}$  is the averaged signal in the time window of  $(0, 0.5)$  ms after the sawtooth. The error bar of SSNPA signals is estimated with the noise observed on the ‘blind’ detector, while the error bar of the neutron rate drop represents the statistical error of neutron measurements. For the tangentially-viewing and radially-viewing SSNPA instruments, each instrument has three arrays with directly deposited foils of different thickness. The corresponding energy threshold for 100 nm, 200 nm and 300 nm foils are  $>25$  keV,  $>45$  keV, and  $>65$  keV respectively. In the discharge 204163, the data were available for only two arrays of the r-SSNPA system due to lack of amplifiers for the third array at that time.

it is possible that an unidentified error in background subtraction also affects the central channels; this would cause an unidentified offset in figure 7(d).

Based on the above measurements from the neutron, SSNPA, and FIDA diagnostics, we can conclude that under the conditions studied here: (1) passing fast ions are strongly expelled from the core to the edge at each sawtooth crash, while trapped fast ions are weakly affected. (2) The redistribution of passing ions occurs in a wide energy range, and no clear energy dependence is observed. These observations are very similar to the phenomenon observed in conventional tokamaks. A strong effect of sawteeth on passing fast ions and a weak/negligible effect on trapped fast ions was observed on TEXTOR with the collective Thomson scattering diagnostic [5], on DIII-D with FIDA diagnostic [6], and ASDEX-Upgrade with FIDA and collective Thomson scattering measurements [7–9]. However, it is worth noting that the observations on NSTX-U do not agree with the most recent MAST measurements and modelling [13], which suggest that both passing and trapped fast ions are redistributed by sawtooth crashes at roughly the same level. There are some differences in the plasma conditions. The magnetic field on NSTX-U is 0.65 T, and the beam injection energy is 72 keV; both are much higher than on MAST. In addition, sawteeth on MAST seem to have no effect on the plasma density evolution, but sawteeth on NSTX-U modulate both the plasma density and temperature. The neutron yield drop at sawtooth crashes on MAST is typically around 30%, while it is only  $<15\%$  on NSTX-U. The

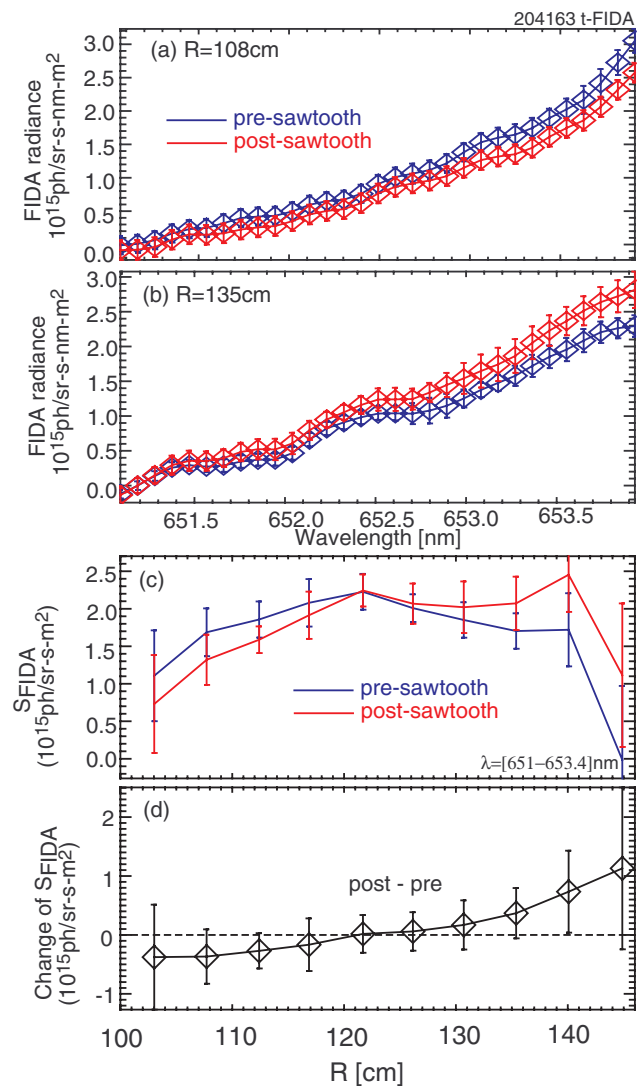


**Figure 7.** Comparison of the t-FIDA spectra before and after sawtooth crashes for (a) a core channel with  $R_{\text{maj}} = 108$  cm and (b) an outer channel with  $R_{\text{maj}} = 135$  cm. (c) Comparison of the t-FIDA spatial profiles before and after sawtooth crashes. (d) Relative change of the t-FIDA radiance before and after sawtooth crashes. The FIDA portion of the spectrum is the Doppler-shifted region with wavelength from 651 nm to 653.4 nm whose corresponding energy along the sightline is 57 keV and 15 keV, respectively. The t-FIDA diagnostic has a spatial resolution of 5 cm. Note the FIDA data are conditionally averaged over several sawtooth events.

physical reason why sawteeth affect fast ions differently on MAST and NSTX-U will be the topic of future study.

### 3. Modelling of sawtooth and comparison with experiments

The time-dependent Tokamak transport code TRANSP [20, 21] is used to simulate sawtooth crashes and calculate the fast ion distribution before and after the sawtooth crashes. The time slices when the sawtooth events occur are specified in an input file. The sawtooth model used in TRANSP can be either the full reconnection Kadomtsev model [10, 11] (with  $NMIX\_KDSAW = 1$  in the TRANSP



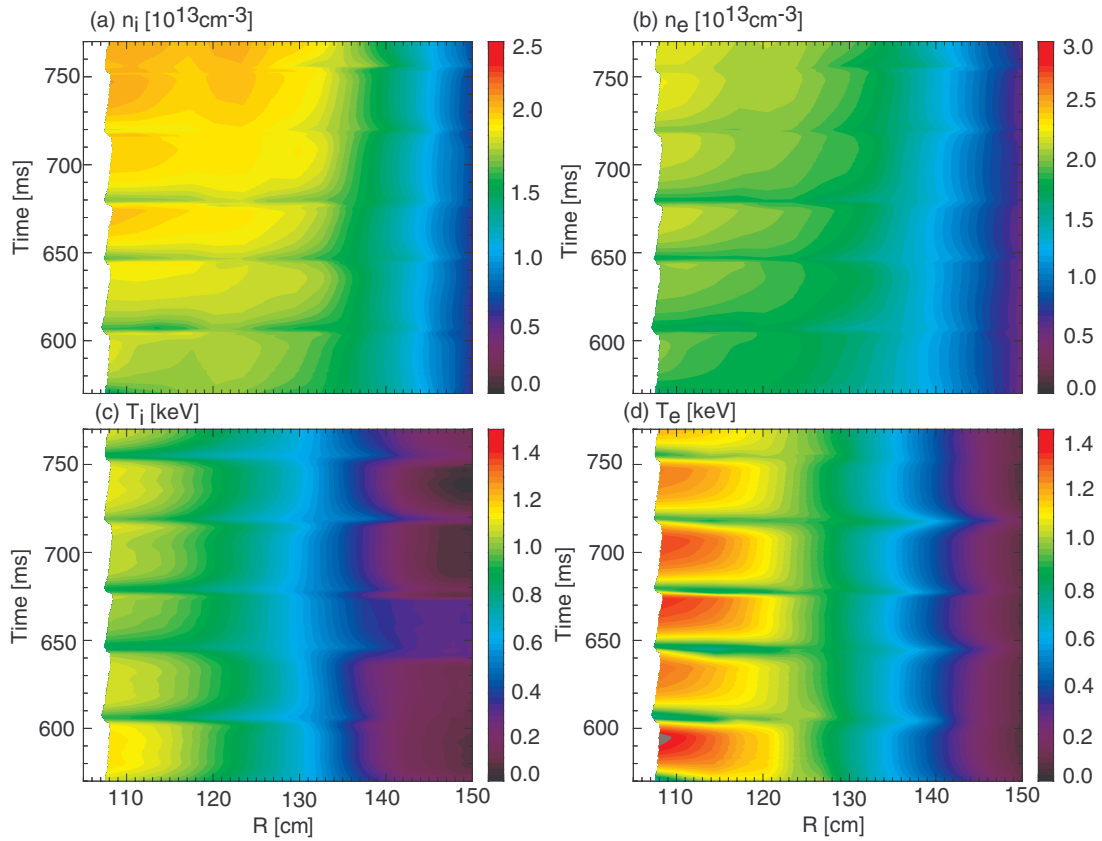


**Figure 8.** Temporal evolution of profiles of (a) thermal ion density, (b) thermal electron density, (c) ion temperature and (d) electron temperature. These profiles are obtained by conditional averaging over all sawtooth events between 0.5 and 1.5 s and are resampled at 1 ms time intervals. They are used as input plasma profiles for the TRANSP sawtooth simulations.

namelist) or partial reconnection Porcelli sawtooth model [22] (with *NMIX\_KDSAW* = 3 in the TRANSP namelist). The Kadomtsev model treats a sawtooth as an ‘internal disruption’ resulting from the nonlinear growth of an  $n = 1$  kink instability. Each pair of surfaces with equal helical flux on the opposite sides of the  $q = 1$  surface reconnect and form a new unified surface with  $q(0) = 1$  and  $q(r) > 1$ . The plasma is mixed between inner/outer flux surfaces with the same helical flux. All the fast ions and thermal ions participating in the mixing are conserved. The Porcelli sawtooth model is a modified Kadomtsev model. The magnetic  $q$  at the magnetic axis rises only part of the way to unity. The magnetic reconnection is partial or incomplete. In the Porcelli sawtooth model, the island width fraction can be specified with the variable *FPORCELLI* in the TRANSP namelist.

A series of TRANSP runs have been performed for the NSTX-U sawtooth discharge 204163. The TRANSP runs are provided with spline fits to experimental plasma profiles. The input experimental profiles are conditionally averaged over all the sawtooth events by aligning them to a single crash time and normalizing them to their value before the sawtooth events. It is assumed that each plasma parameter has a similar temporal evolution for all sawtooth crashes in a short time window just before and after each sawtooth crash. A conditional averaging is needed here because the raw experimental data do not have sufficient temporal resolution for accurate time-dependent sawtooth modelling. The electron density and temperature obtained from the multi-point Thomson scattering (MPTS)

diagnostic have a time resolution of 16.6 ms. The ion density, temperature and toroidal rotation from the charge-exchange recombination spectroscopy (CHERS) diagnostic typically have a time resolution of 10 ms. After conditional averaging, the experimental plasma profiles are resampled on the 1 ms timescale for sawtooth simulation. Figure 8 shows that the plasma density and temperature evolve substantially during a sawtooth cycle. In principle, the rapid change of plasma profile (especially thermal ion density and electron temperature) can affect the neutron emission since the beam-target fusion reaction is proportional to the product of fast ion density and thermal ion density. The first TRANSP/NUBEAM run is used to check how much of the change in neutron emission is due to thermal plasma profile evolution. The sawtooth model is turned on for the  $q$ -profile evolution, but the effect of sawtooth crashes on the fast ion distribution is turned off. Figure 9(a) shows that, as expected, there is a weak modulation in the fast ion density profile. It is interesting to notice that the neutron rate drop caused by thermal plasma profile evolution can be more than 50% of the measured neutron rate drop at a sawtooth crash, see figures 9(b) and (c). In some discharges, the temporal evolution of plasma profiles can account for as much as 90% of the measured neutron rate drop. This is because not only thermal ion density but also beam deposition changes in the sawtooth cycle. Thus, it is important to self-consistently include the changes in plasma profiles in the sawtooth modelling. In the second TRANSP run, the full reconnection Kadomtsev sawtooth model is turned on for both equilibrium

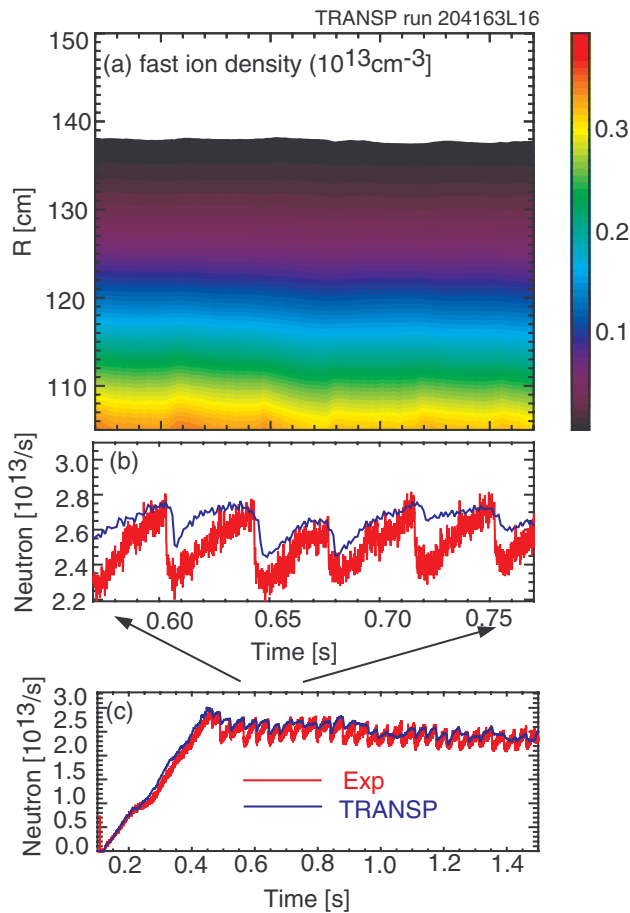


**Figure 9.** (a) Fast ion density and ((b) and (c)) neutron emission calculated by TRANSP simulation 204163L16 in which sawtooth model is turned on for  $q$  profile evolution, but it is turned off for fast ions. The measured neutron rate is shown red curve in panels (b) and (c) for comparison. The TRANSP simulation predicts that the neutron rate drop caused by thermal plasma profile evolution can be as much as 50% of the measured neutron rate drop at the sawtooth crashes.

and fast ions. As suggested in figure 10, the Kadomtsev model always overestimates the neutron rate drops at each sawtooth crash. Even when the fraction of fast ions participating in the sawtooth mixing ( $XSWFRAC\_BEAM$  in the TRANSP namelist) is reduced from 1.0 to 0.5, the predicted neutron emission drop at the sawtooth crashes is still about as large as the experimental data.

Here, it should be noted that the magnitude of the neutron rate from the TRANSP simulation is rescaled by a factor of 0.61 to match the experimental data before  $t = 0.5$  s. The discrepancy in the absolute value also exists in the fast ion confinement experiments in the relatively quiescent plasmas with short beam blips. The discrepancy is partially due to uncertainty in the absolute calibration of the neutron detectors and partially because of the large uncertainty in the effective charge  $Z_{\text{eff}}$  in TRANSP inputs. The same rescaling factor is used in the rest of this paper.

The TRANSP simulations self-consistently solve the poloidal field diffusion equation to evolve the equilibrium and  $q$  profile at sawtooth crash time slices based on the Kadomtsev or Porcelli sawtooth models. The calculated  $q$  profiles are

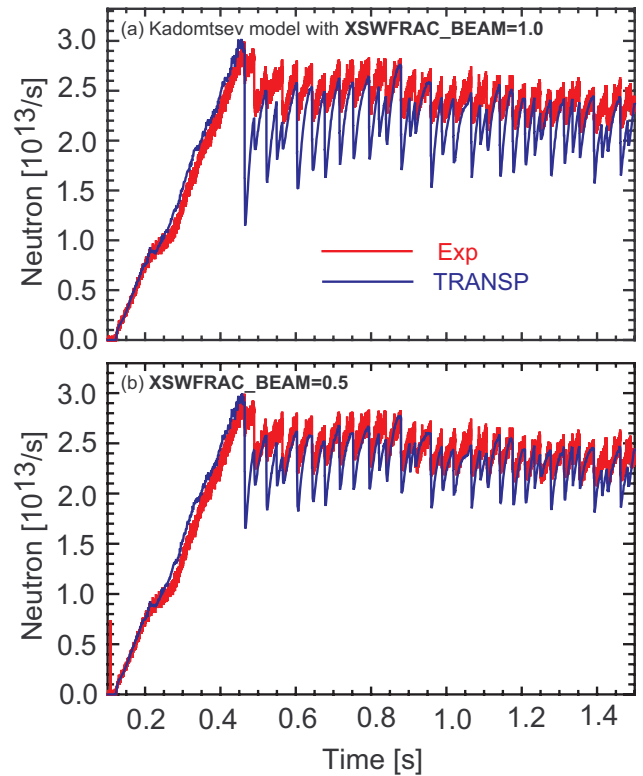


**Figure 10.** TRANSP/NUBEAM calculated neutron emission compared with the measured neutron rate. The full reconnection Kadomtsev sawtooth model is employed in these TRANSP/NUBEAM simulations with (a)  $XSWFRAC\_BEAM = 1.0$  and (b)  $XSWFRAC\_BEAM = 0.5$ , where  $XSWFRAC\_BEAM$  is the fraction of fast ions participating in sawtooth mixing. The full reconnection Kadomtsev sawtooth model overestimates the neutron rate drop at the sawtooth crashes.

shown in figure 11, with the mixing radius about 135 cm and the inversion radius about 127 cm. The inversion radius is pretty close to the experimental value of 123–125 cm, which is inferred from the measurements of soft x-ray emission, electron temperature, and toroidal rotation.

In the third TRANSP simulation, the partial reconnection Porcelli sawtooth model is applied. As shown in figure 12, a good agreement can be obtained between predicted and measured neutron rate when the TRANSP simulation assumes 75% reconnection and 50% fast ions redistributed. The TRANSP calculated neutron rate overlaps with the experimental data and the neutron rate drops at the sawtooth crashes agree well with experimental measurements. The redistribution of fast ion density especially in the core region is also obvious, see figure 12(a). It should be mentioned that the global neutron emission is insensitive to some settings. For example, when the fraction of reconnection is changed from 1.0 to 0.5, the change of the drop of neutron emission at the sawtooth crashes is less than 10%. In the TRANSP simulation, the NUBEAM module is called to calculate and dump out the fast ion distribution every 2 ms in the time windows with sawtooth crashes. Figure 13(a) shows the difference of the spatial distribution of fast ions before (averaged over the time window of (636, 642) ms) and after (averaged over the time window of (644, 650) ms) the sawtooth crash at  $t = 0.643$  s. It shows a strong reduction ( $\approx 20\%$ ) of fast ion density inside the sawtooth

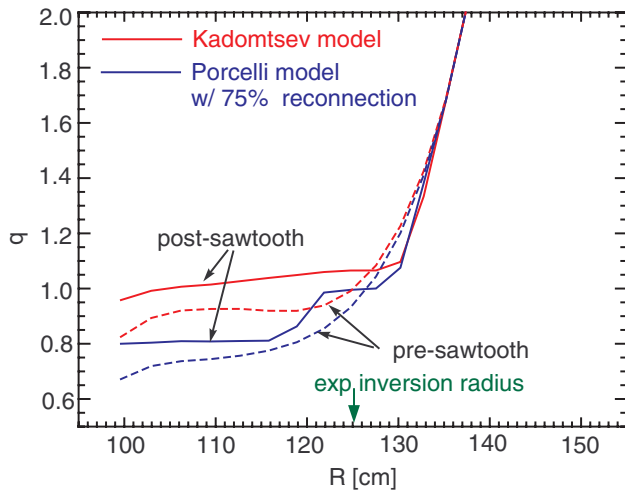


**Figure 11.** Comparison of the TRANSP calculated  $q$  profiles before and after a sawtooth crash. The experimental estimation of the inversion radius is also shown in the plot for comparison. Note that MSE measurements were not available; the inversion radius is inferred from the measurements of electron temperature, soft x-ray emission, and toroidal rotation.

inversion radius and a modest increase (5%–10%) at the edge. Figures 13(b)–(d) compares the difference of the fast ion distribution in the energy/pitch space at three different radial locations. Figure 13(b) shows that fast ions in most pitches in the plasma core are strongly redistributed by sawteeth. At mid-radius (figure 13(c)), some depletion occurs for fast ions with pitch close to 1, but a mixture of increase and reduction occurs in the region with pitch between  $-0.5$  and  $0.5$ . Near the plasma edge (figure 13(c)), there is a significant increase of fast ions in the region with pitch less than  $0.8$  and some reduction of fast ions with pitch close to 1. Figure 13 also shows that fast ions of all energy and in most pitches are affected. This is expected, since the sawtooth models in TRANSP treat all of the particles the same way and do not have any energy and pitch selectivity. Figure 14 compares the radial profile of trapped and passing fast ion density before and after the sawtooth crash. It shows a reduction of passing fast ions in most regions except the very edge. The passing fast ion density in the core is reduced by 15% (see figure 14(b)). The density of trapped particles slightly decreases in the core and increases at  $R > 115$  cm. The relative change of trapped fast ion density is much larger than passing particles although the absolute change is small. The different trend is mainly because the core region is dominated by passing particles, while trapped particles are mainly deposited in the mid-radius. Since the TRANSP sawtooth model conserves the magnetic moment  $\mu$ , some passing particles that move inward to smaller  $R$  convert from passing to trapped orbits.

With the fast ion distributions predicted from the TRANSP simulations, the FIDASIM [36] code is used to calculate synthetic FIDA and SSNPA signals before and after the sawtooth crashes. In order to study the net effects of sawteeth on fast ion distribution, three TRANSP and FIDASIM runs are performed. In the first FIDASIM run, the plasma profiles are evolved but the fast ion distribution is kept the same

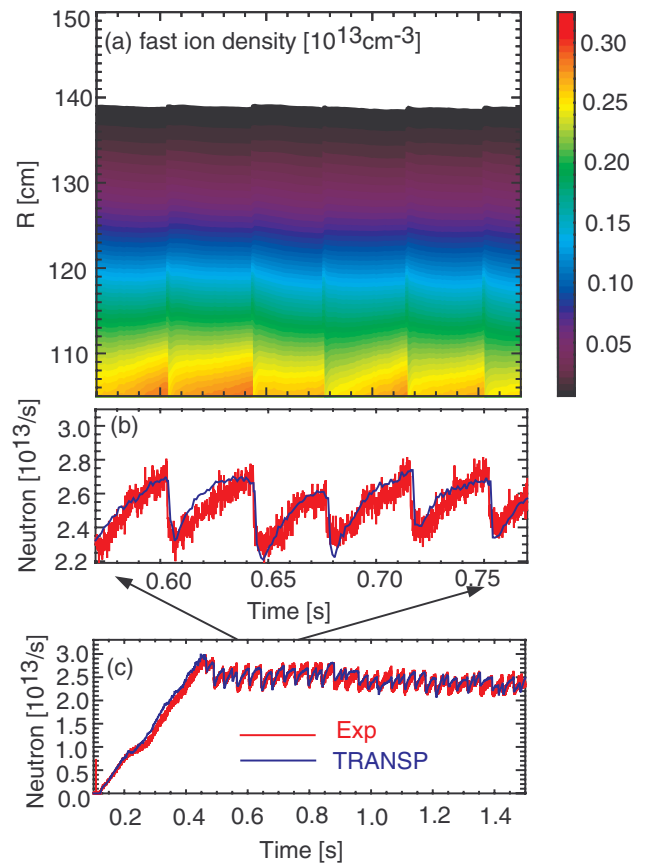


**Figure 12.** (a) Fast ion density and ((b) and (c)) neutron emission calculated by the TRANSP simulation 204163L10 with the partial reconnection Porcelli sawtooth model. The measured neutron rate is also shown as the red curve in panels (b) and (c) for comparison. The predicted neutron emission and neutron drops at the sawtooth crashes agree reasonably well with the measurements.

before and after sawteeth. This is used to check how much the thermal profile changes affect the FIDA signals. As shown in figure 15(a), thermal profile changes alone, without modifying the fast ion distribution, only slightly (3%) increase the FIDA signal in the core region. This suggests that the effect of thermal profile changes on the FIDA spatial profile alone is negligible. In the second TRANSP and FIDASIM run, both the plasma profiles and the fast ion distributions are evolved, but the sawtooth model is turned off for fast ions. In this case, only the thermal ions are redistributed by sawteeth. Fast ion deposition and distribution evolves slowly with the thermal profile change. In the third case, the sawtooth model is turned on for beam ions; both the plasma profiles and fast ion distributions are evolved self-consistently. In the latter two cases, fast ion distributions are generally different at any time slices in the sawtoothing period (see figure 15(c)) because the fast ion distribution function is continuously modified by  $q$  profile evolution and, in case III, by sawteeth. As shown in figure 15(b), in case III, the simulated t-FIDA signals after the sawtooth in most channels are lower than the signals before the sawtooth crash. The reduction of the t-FIDA signals in the core region is mainly because of the transport of fast ion induced by sawteeth. The changes at the outer region with  $R > 115$  cm is most likely because of the thermal plasma

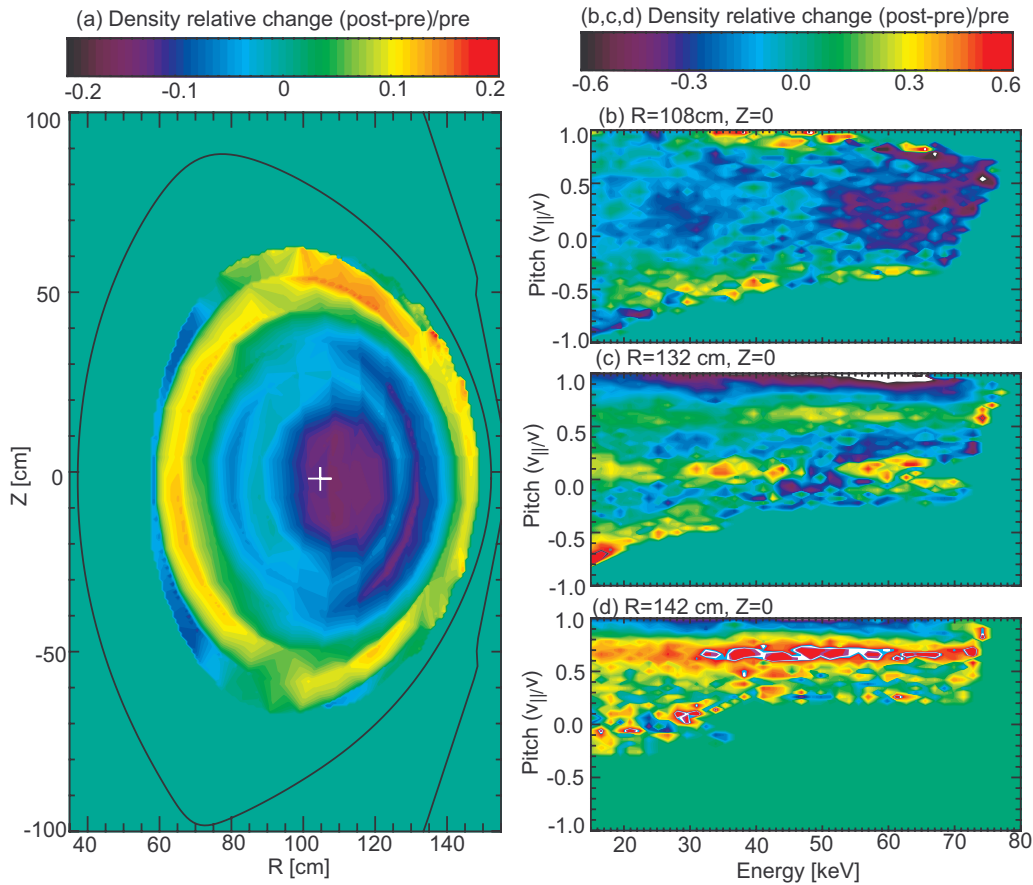


**Figure 13.** Difference of the fast ion distribution function before and after the sawtooth crashes (a) in  $(R, Z)$  space, and in energy/pitch space at (b)  $R = 108$  cm and  $Z = 0$  cm, (c)  $R = 132$  cm and  $Z = 0$  cm, and (d)  $R = 142$  cm and  $Z = 0$  cm. The fast ion distribution is calculated by TRANSP using the partial reconnection Porcelli sawtooth model.

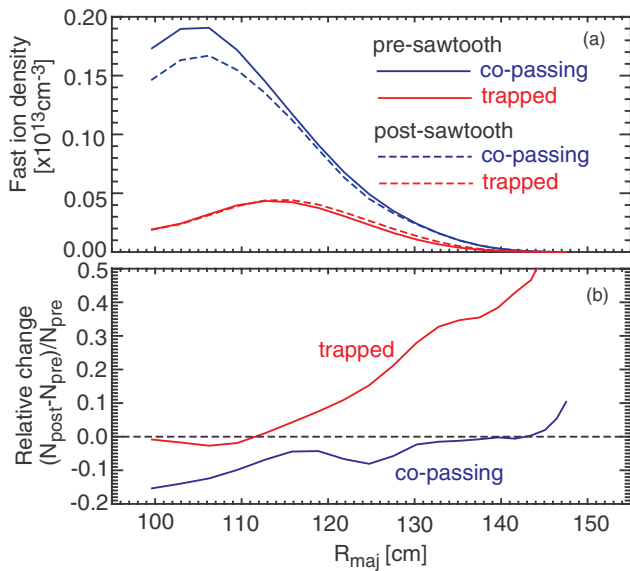


**Figure 14.** Comparison of the spatial profile of trapped and passing fast ion density at outer half of the plasma region before (averaged over the time window of (638–642) ms) and after (averaged over the time window of (644–648) ms) the sawtooth crash. The fast ion density is integrated over all energies. The fast ion distribution is calculated by TRANSP using the partial reconnection Porcelli sawtooth model.

profile evolution and its modification of fast ion deposition. The simulated t-FIDA spatial profile after sawteeth from case II, the dashed dark green curve in figure 15(b), overlaps with the t-FIDA profile before the sawtooth crash in the high field side, and it is lower at the outer region. It is obvious that the FIDASIM simulation results are not entirely consistent with the FIDA experimental measurements: although they predict the reduction of t-FIDA signals in the core region, they fail to predict the signal increase at the edge. The experimental t-FIDA data in figure 7 show that the FIDA signal increases after the sawtooth at outer channels. Readers may be puzzled why the simulated fast ion density increases at the edge after sawteeth (see figure 13(a)), but the simulated t-FIDA signal does not. This is mainly because the t-FIDA is most sensitive to the fast ions with high pitch as indicated in the velocity-space sensitivity function in figure 3(b). Figures 13(b)–(d) shows that the calculated fast ion density decreases in the high pitch region. It is also shown in figure 14 that passing fast ion density decreases in most regions except the very edge after the sawtooth, similar to the simulated t-FIDA spatial profile. The good agreement on neutron rate drop and the discrepancy on the t-FIDA signal change in the outer region highlight the importance of using multiple diagnostics that have different velocity-space sensitivity in the validation of different sawtooth models.

It is challenging to simulate the NPA signal change during the sawtooth crashes and compare with the experimental observations shown in figure 6. Instead, time windows a few ms away from sawtooth crashes are chosen to check how the steady fast ion distribution is affected by the sawtooth. Figure 16(a) shows that the experimental t-SSNPA signal after sawtooth crashes can be 10%–30% higher than the signal before sawtooth crashes. Similarly, the experimental p-SSNPA signal after sawtooth crashes increases 5%–20%. As discussed in section 2, both the t-SSNPA and p-SSNPA measure only passive signals from the plasma edge. The signal increase after sawtooth crashes suggests that some fast particles are redistributed to the outer region where the background neutral density is high. Since the rise of the t-SSNPA signal is larger than the p-SSNPA rise, this indicates that the effect of sawtooth on passing fast ions is stronger. The change of the r-SSNPA signal is the combination of active and passive signals contributions. The opposite trend of the r-SSNPA and p-SSNPA signals indicates that some trapped fast ions leave the plasma core. Figure 16(b) shows that the simulated DC signal of the t-SSNPA and p-SSNPA increases after a sawtooth crash, which qualitatively agrees with the measurements. The discrepancy in the magnitude of the change indicates it likely overestimates the transport of trapped particles and underestimates the transport of passing particles. The different trend in the r-SSNPA data is because of the competition of active signals and passing signals from trapped particles. A more careful check shows that the active signals of the r-SSNPA system actually show a very small decrease, but there is a relatively large increase in the passive signals. In the SSNPA simulations, the changes of fast ion distribution due to thermal profile evolution and the sawtooth are not separated. The SSNPA signals are very localized in energy/pitch space. The simulations suggest that both terms can be important, as in the FIDA simulations. It should be pointed out that, in principle, the changes in the background neutral density could also alter the SSNPA signals. As shown in figure 5(b), the edge neutral density bursts at every sawtooth crash, but it has a minor change a few ms after the sawtooth. The edge neutral density diagnostic (ENDD) [37] measurements also show that the background density profile a few ms after the sawtooth almost overlaps with the profile before the sawtooth. In the SSNPA simulations presented in this work, the background neutral density is calculated by the simple 1D model FRANTIC [38] inside the TRANSP code, and it is almost the same before and after the sawtooth.

The discrepancy between FIDA/SSNPA measurements and FIDASIM simulations may reflect the limits of the sawtooth models in TRANSP. One of the main caveats of Kadomtsev and Porcelli sawtooth models implemented in the TRANSP code is that they treat all the fast ions and thermal ions the same way and they do not include the kinetic effects of fast ions. In other words, fast particles are always attached to a magnetic flux surface, and the fast ions are redistributed according to the rearrangement of flux surfaces at the sawtooth crash. Thus, there is no energy or pitch dependence. Early simulations [39] have shown that full orbit effects may play an important role in a low magnetic field because the cyclotron resonances can enhance

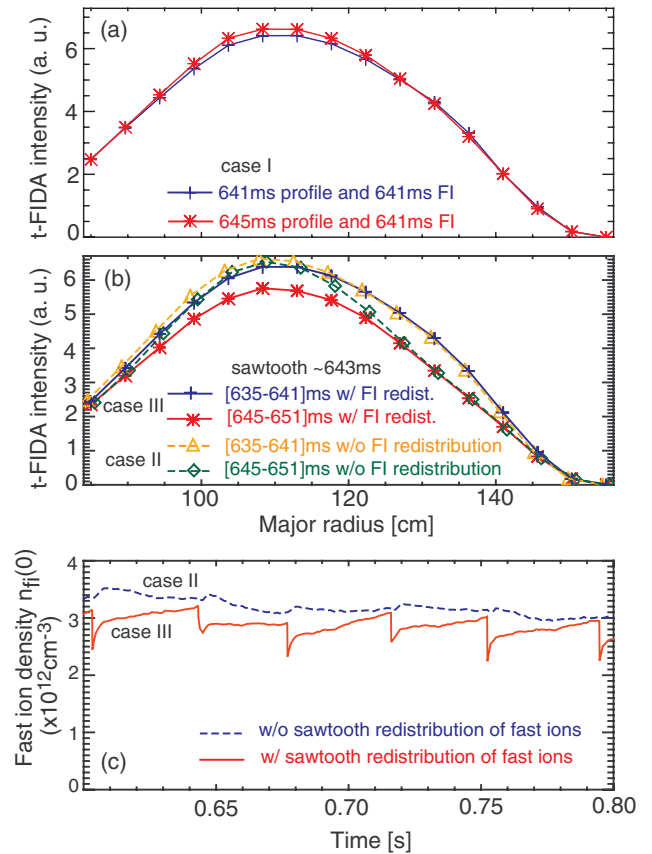


**Figure 15.** Comparison of the simulated t-FIDA spatial profiles before and after the sawtooth around 0.643 s in three FIDASIM cases. (a) Case I: only the thermal plasma profile evolution is considered. The fast ion distribution function before the sawtooth is used in pre-sawtooth and post-sawtooth FIDASIM simulations. (b) Case II and case III: the sawtooth model is turned off for fast ions in case II (see dashed lines), but it is turned on for case III (see solid lines). (c) Comparison of the TRANSP calculated fast ion density in the plasma core in the case II and III. The synthetic t-FIDA signal is calculated by the FIDASIM using the plasma profiles and fast ion distribution from TRANSP using the partial reconnection Porcelli sawtooth model. The t-FIDA spectra are integrated over (651, 653.4) nm, whose corresponding energy range is (15, 57) keV, to get the t-FIDA spatial profile.

the level of stochasticity in fast ion orbits, thereby increasing the extent to which the fast ions are redistributed. In addition, other transport mechanisms, such as the resonant interaction between fast ions and the electromagnetic fields of the sawteeth [25, 40, 41], can also affect fast ions during sawteeth.

The Kadomtsev sawtooth model has been advanced to explain the different effect of sawteeth on passing and trapped fast ions [23, 24, 42]. According to the sawtooth theory in [23, 24], there are three characteristic time scales that determine the property of fast ion transport during a sawtooth crash: (1) the crash duration  $\tau_{cr}$ ; (2) the toroidal precession time  $\tau_{pr}$ ; and (3) longitudinal motion time  $\tau_L$  which is the period around the perturbed flux surface. The toroidal precession tends to keep the particles at a constant minor radius through decorrelation of the particle motion from the sawtooth and phase mixing. The longitudinal motion tends to move the particles along the displaced flux surfaces. If the sawtooth crash is sufficiently fast ( $\tau_{cr} \ll \tau_{pr}$ ), fast ions move together

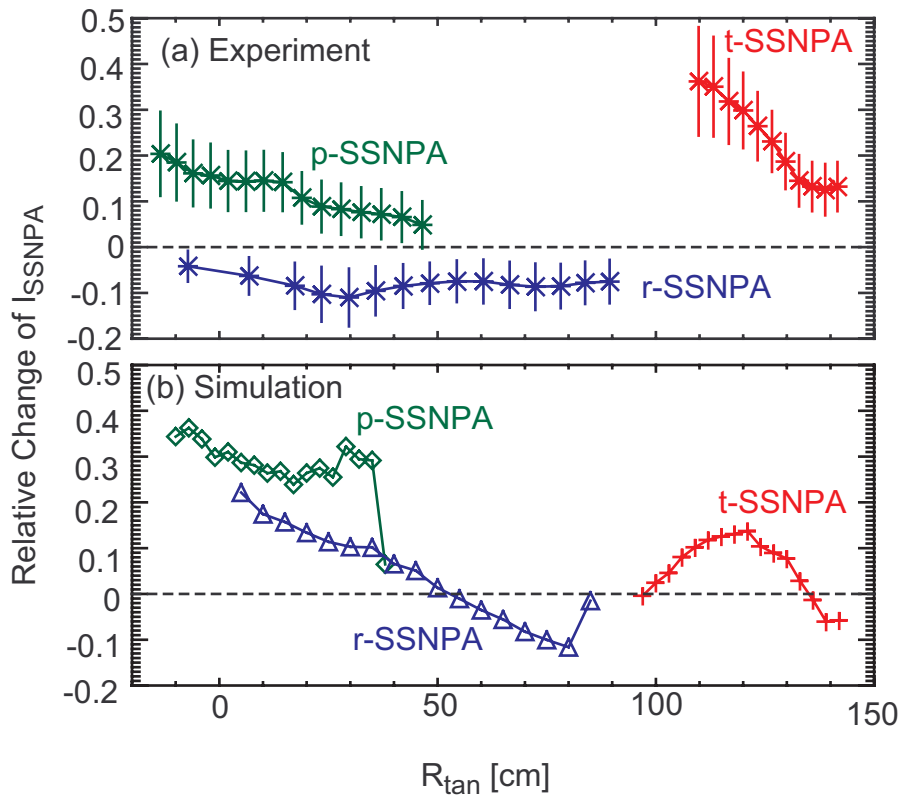


**Figure 16.** Comparison of (a) measurements and (b) simulations of the relative change of the r-SSNPA, t-SSNPA and p-SSNPA signals caused by sawtooth crashes. The relative change of experimental data is defined as  $(S_{\text{post}} - S_{\text{pre}})/S_{\text{pre}}$ , where  $S_{\text{pre}}$  is the averaged signal in the time window  $(-4, 1)$  ms relative to a sawtooth crash time, and  $S_{\text{post}}$  is the averaged signal in the time window  $(3, 6)$  ms relative to the sawtooth crash time. The experimental error bars are estimated with the standard deviation of relative change of all sawtooth events in the discharge 204163 between 0.5 and 1.5 s. The simulation is performed for all the SSNPA systems at  $t = 0.639$  s and  $t = 0.645$  s, and the sawtooth time is around 0.643 s.

with the evolving flux surfaces, and this leads to significant fast ion transport. However, when  $\tau_{\text{pr}} < \tau_{\text{cr}}$ , the influence of sawtooth crash on a particle's dynamics depends on the competition of  $\tau_{\text{pr}}$  and  $\tau_{\text{L}}$ . Strong fast ion transport can still occur when  $\tau_{\text{pr}} \gg \tau_{\text{L}}$ . The conditions for strong redistribution are  $\tau_{\text{cr}} \ll \tau_{\text{pr}}$  and  $\tau_{\text{L}} \ll \tau_{\text{pr}}$ , and they can be expressed in energy and pitch. In other words, there exists a pitch-dependent critical energy  $E_{\text{crit}}$ . The particles with energy less than  $E_{\text{crit}}$  are strongly redistributed at the sawtooth crash. The longitudinal motion time  $\tau_{\text{L}}$  is obtained from equation (10) in [24], i.e.  $\tau_{\text{L}} \simeq \tau_{\text{pr}}/|q - 1|$  for trapped particles and  $\tau_{\text{L}} \simeq \tau_{\text{bounce}}/|q - 1|$  for passing particles. The condition  $\tau_{\text{cr}} = \tau_{\text{pr}}$  gives the critical velocity (equation (11) in [24]) and critical energy for trapped particles  $E_{\text{crit}} = 2\pi m_i \kappa r R_0 \omega_B / \tau_{\text{cr}}$ , where  $m_i$  is the ion mass,  $\kappa$  is the ellipticity, and  $\omega_B$  is the ion cyclotron frequency. The critical velocity for passing fast ions can be obtained with equation (13) in [24]. The toroidal precession time  $\tau_{\text{pr}}$  is calculated numerically by a guiding-center code with the conservation of energy, magnetic moment and canonical toroidal momentum. For the discharge 204163 shown in this paper, beam injection energy is 72 keV, and the sawtooth crash time is around 40–50  $\mu\text{s}$  based on the soft x-ray emission. Based on equations (11) and (13) in [24], the critical energies are about 65 keV for well circulating (with pitch  $V_{\parallel}/v$  of 0.9–1.0) and 25–30 keV for trapped particles. The calculation of  $E_{\text{crit}}$  qualitatively reproduces the observed results that a large population

of passing particles is strongly redistributed by sawteeth and trapped particles are weakly affected.

#### 4. Summary





Repetitive sawteeth are observed in long L-mode discharges on the NSTX-U in the 2016 run campaign. These sawtooth crashes can result in neutron rate drops as large as 15%, followed by an increase of edge  $D_{\alpha}$  light. The temporal evolution of plasma profiles can account for more than 50% of the measured neutron rate drop at the sawtooth crashes. Changes of fast ion diagnostic signals are strongly correlated with the sawtooth events. Analysis of the signal changes of three SSNPA instruments shows that passing fast ions in the whole detectable energy range are strongly redistributed from the plasma core to the plasma edge, but trapped particles are weakly affected. This observation is also confirmed by the tangential- and vertical-FIDA measurements. This observation is very similar to what has been seen in the conventional high field and large aspect ratio tokamaks, but it is different from the measurements and modeling results on MAST. The observed difference in the transport of passing and trapped particles can be explained by calculations of the pitch-dependent critical energies for strong redistribution. The full connection Kadomtsev and partial reconnection Porcelli sawtooth models within the

TRANSP code have been used to simulate the sawteeth on NSXT-U. The Kadomtsev model generally overestimates the sawtooth drops at the sawtooth crashes. When tuning the input parameters, the Porcelli model can reproduce the neutron rate drops and FIDA signal drops in the core region, but it fails to produce the FIDA signal increase at the edge. The SSNPA simulation results partially agrees with the measurements, and also suggest that the sawtooth model overestimates the transport of trapped particles and underestimates the transport of passing particles. There are several caveats of the present sawtooth models in TRANSP: (1) passing and trapped particles are treated the same way, (2) FLR effect was not considered. A new sawtooth model is being developed to include energy and pitch selectivity in TRANSP [43]. Initial results recover the increase of fast ion density across the inversion radius. Also, the Kadomtsev sawtooth mixing model is being further generalized [44]; and a first-principle code is being used to simulate sawteeth and related fast ion transport [45]. These new capabilities, flexible neutral injection geometry and more fast ion diagnostics in the coming NSTX-U run campaigns will enable more quantitative comparison between measurements and theory on the effect of sawtooth on fast ions, background MHD and impurity transport, and help sawtooth model development and validation in a wide range of plasma parameters.

## Acknowledgments

The authors would like to thank for the contribution of the whole NSTX-U team as well as the helpful discussions with Dr R.E. Bell on the CHERS data, Dr F. Scotti on the edge  $D_{\alpha}$  measurements and Dr K. Tritz on the soft x-ray data. This work is supported by the US DOE under DE-AC02-09CH11466, DE-FG02-06ER54867 and DE-FG03-02ER54681. The digital data of this paper can be found at <http://dataspace.princeton.edu/jspui/handle/88435/dsp011v53k0334>.

## ORCID iDs

D. Liu  <https://orcid.org/0000-0001-9174-7078>  
 M. Podestà  <https://orcid.org/0000-0003-4975-0585>  
 G.Z. Hao  <https://orcid.org/0000-0003-2310-6134>  
 D. Kim  <https://orcid.org/0000-0002-6085-9525>

## References

- [1] Von Goeler S., Stodiek W. and Sauthoff N. 1974 *Phys. Rev. Lett.* **33** 1201–3
- [2] Sauter O. et al 2002 *Phys. Rev. Lett.* **88** 105001
- [3] Lovberg J.A., Heidbrink W.W., Strachan J.D. and Zaveryaev V.S. 1989 *Phys. Fluids B* **1** 874–92
- [4] Marcus F.B. et al 1991 *Plasma Phys. Control. Fusion* **33** 277
- [5] Nielsen S.K. et al 2010 *Plasma Phys. Control. Fusion* **52** 092001
- [6] Muscatello C.M., Heidbrink W.W., Kolesnichenko Y.I., Lutsenko V.V., Zeeland M.A.V. and Yakovenko Y.V. 2012 *Plasma Phys. Control. Fusion* **54** 025006
- [7] Geiger B. et al 2014 *Nucl. Fusion* **54** 022005
- [8] Geiger B. et al 2015 *Plasma Phys. Control. Fusion* **57** 014018
- [9] Rasmussen J. et al 2016 *Nucl. Fusion* **56** 112014
- [10] Kadomtsev B.B. 1975 *Fiz. Plasmy* **1** 710
- [11] Kadomtsev B.B. 1975 *Sov. J. Plasma. Phys.* **1** 389
- [12] Ceconello M. et al 2015 *Plasma Phys. Control. Fusion* **57** 014006
- [13] Ceconello M., Sperduti A. and The MAST Team 2018 *Plasma Phys. Control. Fusion* **60** 055008
- [14] Ono M. et al 2000 *Nucl. Fusion* **40** 557
- [15] Menard J. et al 2012 *Nucl. Fusion* **52** 083015
- [16] Gerhardt S., Andre R. and Menard J. 2012 *Nucl. Fusion* **52** 083020
- [17] Ono M. et al 2015 *Nucl. Fusion* **55** 073007
- [18] Menard J. et al 2017 *Nucl. Fusion* **57** 102006
- [19] Boyer M. et al 2018 *Nucl. Fusion* **58** 036016
- [20] Hawryluk R. 1980 *Physics of Plasmas Close to Thermonuclear Conditions* vol 1, ed B. Coppi et al (Brussels: CEC) pp 19–46
- [21] Pankin A., McCune D., Andre R., Bateman G. and Kritz A. 2004 *Comput. Phys. Commun.* **159** 157–84
- [22] Porcelli F., Boucher D. and Rosenbluth M.N. 1996 *Plasma Phys. Control. Fusion* **38** 2163
- [23] Kolesnichenko Y.I. and Yakovenko Y.V. 1996 *Nucl. Fusion* **36** 159
- [24] Kolesnichenko Y.I., Lutsenko V.V., Yakovenko Y.V. and Kamelander G. 1997 *Phys. Plasmas* **4** 2544–54
- [25] Kolesnichenko Y.I., Lutsenko V.V., White R.B. and Yakovenko Y.V. 2000 *Nucl. Fusion* **40** 1325
- [26] Liu D., Heidbrink W.W., Tritz K., Zhu Y.B., Roquemore A.L. and Medley S.S. 2014 *Rev. Sci. Instrum.* **85** 11E105
- [27] Liu D., Heidbrink W.W., Tritz K., Fredrickson E.D., Hao G.Z. and Zhu Y.B. 2016 *Rev. Sci. Instrum.* **87** 11D803
- [28] Podesta M., Heidbrink W.W., Bell R.E. and Feder R. 2008 *Rev. Sci. Instrum.* **79** 10E521
- [29] Bortolon A., Heidbrink W.W. and Podesta M. 2010 *Rev. Sci. Instrum.* **81** 10D728
- [30] Darrow D.S. 2008 *Rev. Sci. Instrum.* **79** 023502
- [31] Darrow D.S. 2017 *Fusion Sci. Technol.* **71** 201–6
- [32] Boeglin W.U., Perez R.V. and Darrow D.S. 2010 *Rev. Sci. Instrum.* **81** 10D301
- [33] Netepenko A., Boeglin W.U., Darrow D.S., Ellis R. and Sibilia M.J. 2016 *Rev. Sci. Instrum.* **87** 11D805
- [34] Heidbrink W.W. 2010 *Rev. Sci. Instrum.* **81** 10D727
- [35] Hao G.Z., Heidbrink W.W., Liu D., Stagner L., Podesta M., Bell R.E. and Bortolon A. 2018 *Rev. Sci. Instrum.* **88** accepted
- [36] Heidbrink W.W., Liu D., Luo Y., Ruskov E. and Geiger B. 2011 *Commun. Comput. Phys.* **10** 716–41
- [37] Stotler D.P., Scotti F., Bell R.E., Diallo A., LeBlanc B.P., Podestà M., Roquemore A.L. and Ross P.W. 2015 *Phys. Plasmas* **22** 082506
- [38] Tamor S. 1981 *J. Comput. Phys.* **40** 104–19
- [39] Yakovenko Y.V., Kolesnichenko Y.I., Lutsenko V.V., Burdo O.S. and White R.B. 2006 *Proc. 21st IAEA Fusion Energy Conf. (Chengdu, China, 2006)* ([www-pub.iaea.org/mtcd/meetings/fec2006/th\\_p6-6.pdf](http://www-pub.iaea.org/mtcd/meetings/fec2006/th_p6-6.pdf))
- [40] Kolesnichenko Y.I., Lutsenko V.V., White R.B. and Yakovenko Y.V. 1998 *Phys. Plasmas* **5** 2963–76
- [41] Kolesnichenko Y.I., Lutsenko V.V. and Yakovenko Y.V. 1998 *Phys. Plasmas* **5** 729–34
- [42] Gorelenkov N.N., Budny R.V., Duong H.H., Fisher R.K., Medley S.S., Petrov M.P. and Redi M.H. 1997 *Nucl. Fusion* **37** 1053
- [43] Kim D., Podesta M., Liu D. and Poli F.M. 2018 *Nucl. Fusion* **58** 082029
- [44] Mironov M.I., Zaitsev F., Gorelenkov N., Petrov M., Afanasyev V. and Mironov M. 2018 *Nucl. Fusion* **58** 082030
- [45] Shen W., Fu G.Y., Sheng Z.M., Breslau J.A. and Wang F. 2014 *Phys. Plasmas* **21** 092514